Size distribution of silica nanoparticles

Dutka, M. V.; Turkin, A. A.; Vainchtein, D. I.; Gersen, S.; Van Essen, V. M.; Visser, P.; Mokhov, A. V.; Levinsky, H. B.; De Hosson, J. Th. M.

Published in:
Functional Nanostructures

DOI:
10.24274/fn.2016.a1

Publication date:
2016

ONECENTRAL PRESS

Available online at www.onecentralpress.com

One Central Press

journal homepage: www.onecentralpress.com/functional-nanostructures

Size distribution of silica nanoparticles: its impact on green energy

M. V. Dutka,[1] A. A. Turkin,[2] D. I. Vainchtein,[1] S. Gersen,[3] V. M. van Essen,[3] P. Visser,[3] A. V. Mokhov,[4] H. B. Levinsky,[3,4] and J. Th. M. De Hosson[1]

[1]*Department of Applied Physics, Zernike Institute for Advances Materials, University of Groningen, Nijenborgh 4, 9747 AG Groningen, The Netherlands. E-mail address corresponding author: Jeff Th M De Hossson: nanostructures@rug.nl*
[2]*National Science Center "Kharkiv Institute of Physics & Technology," Akademichna str. 1, UA-61108 Kharkiv, Ukraine*
[3]*DNV KEMA Energy & Sustainability, Nederland B.V., P.O. Box 2029, 9704 CA Groningen, The Netherlands*
[4]*Laboratory for High Temperature Energy Conversion Processes, University of Groningen, Nijenborgh 4, 9747 AG Groningen, The Netherlands*

ABSTRACT

The kinetics of formation of silica fractal-like aggregates during combustion of a stoichiometric methane/air mixture with the hexamethyldisiloxane admixture is studied. Oxidation of hexamethyldisiloxane proceeds very fast with formation of SiO_2 molecules and compact silica clusters at a height of a few millimeters above the burner. At a sufficiently high concentration of hexamethyldisiloxane random collisions of nanoparticles leads to agglomerates with fractal-like structure. The transmission electron microscopy is combined with the theoretical analysis to find conditions for formation of silica fractal-like aggregates. The onset of fractal aggregate formation is discussed by studying the characteristic time scales of collisions and coalescence. One dimensional model is formulated to describe the evolution of the size distribution of fractal-like silica particles undergoing generation, convection, sintering and Smoluchowski coagulation. The simulation results are compared to experimental data.

I. INTRODUCTION

Nanoparticles can be produced naturally nearly in every flame. Today this phenomenon is used for gas phase combustion synthesis of a variety of inorganic oxides in the form of fine particles amounting to millions of tons annually [1]. They are used industrially as pigments, opacities, catalysts etc. Experimental, modeling and industrial aspects of particle formation in flames can be found in review papers [2-7]. However, in many combustion applications, such as in domestic boilers or gas engines formation of particles during combustion is undesirable. The growing consumption of silicones and siloxanes and the subsequent increased concentration found in wastewater, together with the increasing interest in the production of biogas and "green energy" in sewage treatment plants, has created significant concern about the presence of siloxanes in biogas [8]. When using biogas as an energy source, during combustion, siloxanes are converted into silica particles which deposit onto internal parts of the equipment and are emitted into the environment [9-14]. Clogging of equipment by silica particles can result in premature equipment failure. The thickness and density of deposited silica layers depends on particle morphology and particle size distribution (PSD). Direct use of biogas at production sites may lead to significant problems related to siloxanes. According to Urban et al.[15] the concentration of hexamethyldisiloxane ($C_6H_{18}Si_2O$, denoted as L2) in landfill gas can reach values as high as 1449 mg/m^3 or 200 ppmv (in the following ppmv ≡ ppm). When biogas is injected into natural gas grids the impurities are become diluted. However, at the moment there is no generally accepted requirement for limiting siloxane concentration in biogas. Siloxane limits from several manufacturers are listed in Ref. 9. According to report [16] devoted to challenges and aims of a European standard on biomethane for grid injection and use as a fuel, in the European countries no regular studies have been carried out in order to define precisely a threshold of siloxanes in biomethane. Because of the growing trend towards the introduction of biogases in the natural gas grid the development of well grounded siloxane/silicon specifications for gas utilization equipment are needed. To develop specifications based on a physically correct basis, fundamental knowledge on silica particle formation in flames is essential.

In this paper we analyze the kinetics of formation of silica fractal-like aggregates during combustion of a premixed stoichiometric methane/air mixture with L2 admixture. In our experiments with the perforated ceramic tile burner we have

found that the oxidation of L2 proceeds very fast with formation of SiO_2 molecules and compact silica clusters at a height of a few millimeters above the burner deck [17]. When travelling through the flame the silica particles grow due to collisions. At a sufficiently high concentration of L2 random aggregation of nanoparticles leads to agglomerates with fractal-like structure. Below we combine the transmission electron microscopy (TEM) measurements with the theoretical analysis to find conditions for formation of silica fractal aggregates. TEM is used to evaluate size and morphology of silica nanoparticles depending on position in the flame above the burner. The model presented in Sec. III is based on a mean-field description of PSD evolution via the Smoluchowski coagulation [18,19]. Colliding nanoparticles often form dendritic fractal-like structures [19-24] if coalescence or sintering of nanoparticles is a slow process. The onset of fractal-like aggregate formation is discussed below by studying the characteristic time scales of particle collisions and sintering. A new expression for the silica sintering time based on the Doremus model [25,26] of viscosity of amorphous materials is proposed. Evolution of a population of non-spherical aggregates of primary particles driven by collisions and sintering can be described by a two-dimensional kinetic equation for PSD using volume and surface area of particles as independent variables [27-29]. In this paper we use one-dimensional approach. The advantage of the one-dimensional model is that it describes the PSD evolution with a good accuracy and for a very low computational cost. To take into account sintering of particles inside the fractal-like aggregates, we use the phenomenological dependence of primary particle radius on distance from the burner and modify accordingly our previous one-dimensional model [30]. Fractal-like aggregates of primary particles is characterized by a fractal dimension [31,32] $D_f < 3$ In our model we use the concept of an effective collision radius of a fractal-like particle [33,34]. The fractal dimension is assumed to depend on number and size of primary particles in aggregates. The simulation results are compared to experimental data.

II. EXPERIMENTAL

A schematic of the experimental setup is shown in Fig. 1. It has two main parts: the gas handling system and the sampling system. The former is used to create gas mixture of air, methane and siloxane and feed it to a burner. To add L2-siloxane to the gas mixture the methane flow is divided into two parts. One part goes through custom made pressure resistant gas bubblers containing hexamethyldisiloxane L2 and then two parts of fuel are mixed with air [13].

The silica particles and aggregates are produced in a flat flame obtained in a burner with perforated ceramic plate [35] with diameter of 60 mm and pore size of 1 mm. The total mass flux of the stoichiometric methane/air mixture was ρv = 0.28 kg/(m^{2}s), which is equivalent to an exit velocity of 0.25 m/s of the unburned mixture.

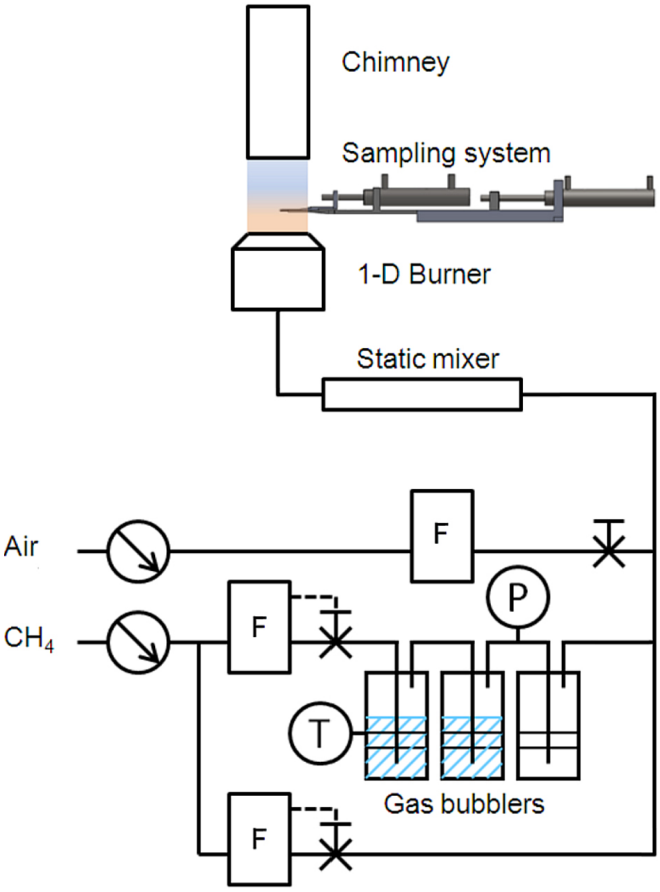

Figure 1 Experimental setup: P – pressure gauge, F – flow meter, FC – flow controller, T – temperature meter, M – manual valve, R – reducer.

In our study we used the stoichiometric flame because of experimental convenience. The kinetics of formation of silica nanoparticles and aggregates in flames is controlled merely by collisions of silica particles in flue gases rather than the deviation in stoichiometric proportion in methane/nitrogen/oxygen mixture. The most important parameters governing evolution of the particle ensemble are the flame temperature and silicon mole fraction in the combustion products. The flame temperature was varied by changing heat loses to the burner head. The temperature of the flame was in the range from 2000 K to 2100 K that corresponds to the adiabatic lean flame at equivalence ratio of 0.8. The axial flame temperature profile (Fig. 2) was determined experimentally with an accuracy of 50 K by using spontaneous Raman spectroscopy [36-38]. The measured flame temperature reaches maximum values at a short distance from the burner deck and then gradually decreases downstream.

We followed a study of Lee et al. [41] to fabricate the thermophoretic probe. Lee et al. [41] reviewed thermophoretic sampling techniques and proposed an improved design for sampling with high spatial resolution. Lee et al. [41] have shown that probe construction can significantly affect the

precision of particle sampling in flame. Approach of Lee et al. [41] with modifications described below allowed us to make an efficient probe that minimally disturbs the flame when collecting particles.

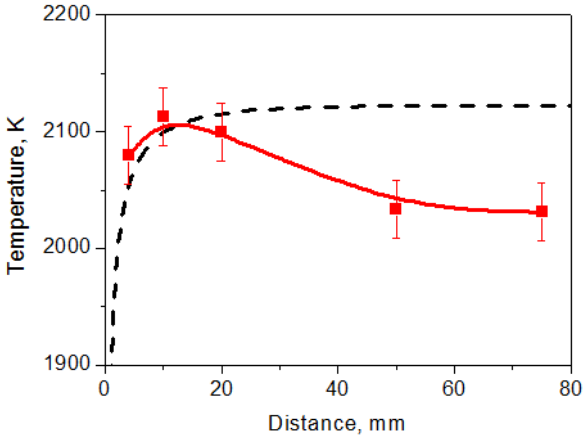

Figure 2 Temperature profiles in stoichiometric laminar premixed methane/air flame. Measured profile is shown with symbols. The calculated profile (dashed line) was obtained by solving a set of equations describing one-dimensional flames using the PREMIX code from the Chemkin II suite [39] and using the GRI 3.0 chemical mechanism. [40]

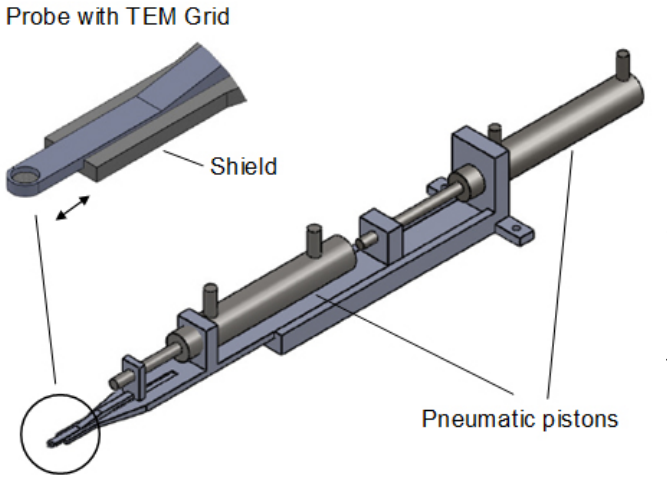

Figure 3 The sampling system with two nitrogen-driven pneumatic pistons.

Initially we tested two types of the probe. The first type (Fig. 4(a)) had one opening with diameter of 2.3 mm and an indent of 3.1 mm from the top for the TEM grid. A distance from the grid to the bottom of the probe was 1 mm. The second type (Fig. 4(b)) had two additional 3.1 mm openings on both sides of the grid. The distance from the grid to the bottom of the probe was reduced to 0.2 mm.

Multiple sampling experiments at L2 concentration of 2700 ppm (the L2 concentration is measured in the unburned fuel/air mixture) with the first type of the probe showed neither considerable morphology nor concentration difference among measurements at various heights (Figs. 4(c) and 4(e)). In contrast, substantially increased amount of material was collected by sampling with the second probe (Figs. 4(d) and 4(f)). Based on these measurements all our experiments have been made with the second probe.

As can be seen in Figs. 4(d) and 4(f), the concentration of particles is too high for quantitative image analysis, therefore a reduced L2 concentration was used for investigation of particles growth.

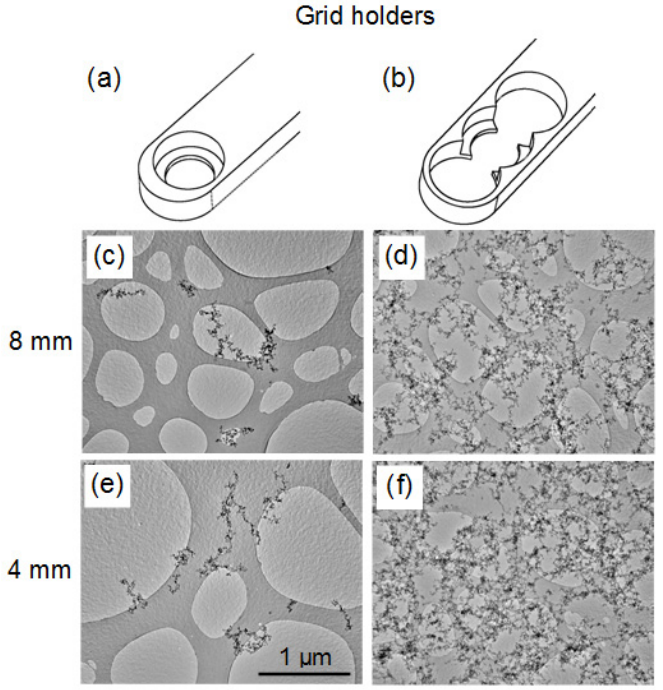

Figure 4 Schematics of thermophoretic probes (a) and (b) and TEM micrographs showing collected silica aggregates formed at different heights above the burner with L2 concentration 2700 ppm.

The experiments were performed at low and high concentrations of L2, i.e. at 50 ppm and 270 ppm, respectively. An electronic circuit capable of producing pulses of duration 50 to 1000 ms controls the solenoid valves used to relay pressure to the pneumatic cylinders. A 100 MHz digital oscilloscope Agilent 54622A was used to determine the pulse duration that was assumed to be equal to the sampling time. To study the particle growth at different positions in the flame the burner was moved vertically along the sampling system with a precision of 0.1 mm. The sampling was performed at heights 6, 8, 10, 15, 30, 50 and 75 mm above the burner deck. Sampling times were selected so that collected silica aggregates do not overlap on the TEM grid. At the high concentration, the sampling time was 100 ms. At the low concentration the sampling time of 500 ms was used in order to get amount of aggregates approximately equal to that at the high concentration.

Under our experimental conditions the main mechanism governing deposition of silica particles on the probe is the thermophoresis [42]. The short traveling time of the particle from the high temperature zone to the cold probe and independence of thermophoretic velocity upon the size of particles [13,43-46] guarantee similarity of particles distribution on the grid with that in the flame. To evaluate the influence of collisions with the grid surface on formation of aggregates we performed experiments with two different types of sampling: horizontal sampling and vertical

one when the TEM grid is parallel to the flow of combustion products. The concentration of aggregates collected during horizontal sampling was higher, while morphology size distribution of aggregates collected by two methods was similar, which indicates that the chosen experimental technique had no significant influence on the aggregate formation.

Transmission electron microscopy has been used to study the morphology of silica aggregates. TEM micrographs of samples collected at different heights were obtained with a Jeol 2010F microscope operated at 200 kV. Sufficient number of images was acquired to allow the characterization of more than 150 individual aggregates per sample. Chemical composition of collected particles was measured by Bruker QUANTAX EDX microanalysis system for TEM. Quantitative analysis of EDX spectra confirmed that composition of particles corresponds to SiO_2.

Image pre-processing and analysis were performed using MATLAB software package following closely the procedures described in literature [17,47,48]. Aggregates that touch edges of images were excluded from the analysis, as there were aggregates having too low contrast to the background. Obtained binary images were analyzed using a custom-written MATLAB code. The code allows us to determine automatically the projected area of agglomerate, its maximum projected length L and width W in the direction perpendicular to L. Diameters of primary particles d_p and their positions with respect to the geometric center of the agglomerate were measured for each aggregate. The aggregates with unidentified primary particles were rejected from the analysis.

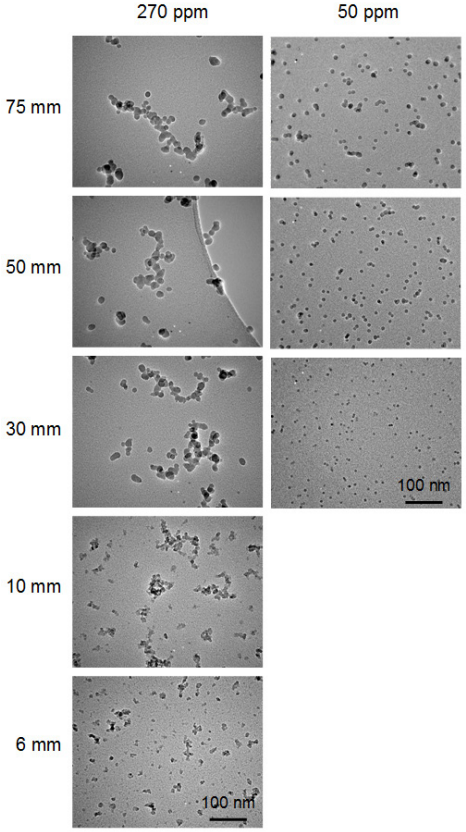

Figure 5 Dependence of the silica particle morphology on concentration and distance from the burner.

TEM micrographs illustrating morphology of silica particles and its dependence on L2 concentration and the distance from the burner surface are shown in Fig. 5. At the high concentration of L2 at the position of 6 mm a high number of single particles is present; and most of the aggregates consisted only of a few particles. At the distance of 10 mm and higher from the burner the dendrite structures with a high number of primary particles are typically present, with almost no single particles.

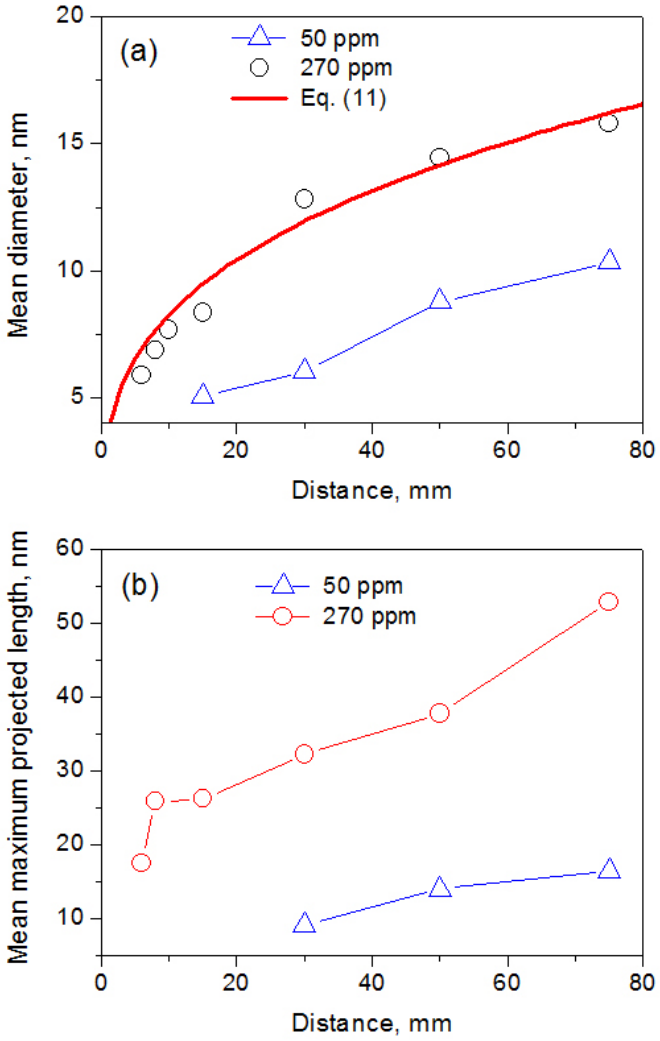

Figure 6 (a) The mean diameter of primary particles $\overline{d}_p$ as a function of distance from the burner deck at low (50 ppm) and high (270 ppm) concentrations of L2. The solid line is the fitting dependence (11). (b) The mean maximum projected length $\overline{L}$ as a function of the distance from the burner deck at low (50 ppm) and high (270 ppm) concentrations of L2.

Image analysis for the low concentration of L2 was only possible to perform with samples collected at the distance of 30 mm or higher. At distance of 15 mm particle-to-background contrast in TEM micrograph was unsuitable for analysis, besides at lower distances particles were too small to be visible by TEM. The resolution of the microscope used for TEM analysis is about 0.1 nm. However, the combination of 20 nm thick supporting amorphous carbon film and amorphous silica aggregates on the

top of it decreases the image contrast, and makes it impossible to distinguish the silica particles less than ~1-2 nm. For this reason the EDX analysis was used to confirm the presence of Si on the areas, where no particles have been visible by the TEM. At the distance of 30 mm most of the collected particles were globular, i.e. consisted of single primary particles. At the distance of 75 mm the concentration of single particles was still high, though aggregates consisted of several primary particles were also seen. The dependence of the mean diameters of primary particles $\overline{d}_p$ and the mean maximum projected length $\overline{L}$ on height is shown in Fig. 6.

The fractal dimension of collected aggregates was determined using the relation[32]

$$N_p = k_0 \left(\frac{\sqrt{LW}}{d_p} \right)^{D_f}, \quad (1)$$

where N_p is the number of primary particles in the aggregate and k_0 is a numerical factor. The fractal dimension is found by linear fitting of N_p to the ratio in the right hand side of (1) in the double logarithmic scale. An example of fractal dimension determination for particles collected at 30 mm at L2 concentration of 270 ppm is demonstrated in Fig. 7. The fractal dimension D_f decreases monotonically downstream from 1.92 to 1.85 (Fig. 7(b)).

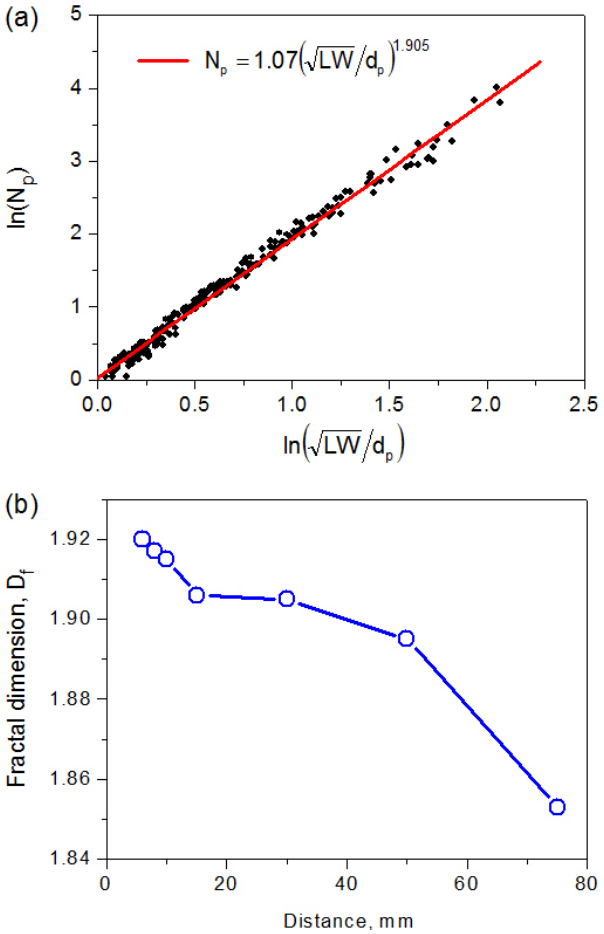

Figure 7 (a) Determination of aggregate fractal dimension (height 30 mm, L2 concentration 270 ppm); the solid line is the fitting function $N_p = 1.07\left(\sqrt{LW}/d_p\right)^{1.905}$. (b) The dependence of fractal dimension on distance from the burner.

III. MODEL

It is well known that the oxidation of methane is mainly taking place in the flame front, very close to the burner surface, in a sequential process involving many intermediate reactive species [49]. As mentioned above small amounts of L2 is added to methane, which is oxidized rapidly near the burner surface [17]. We did not investigated in detail the oxidation kinetics of L2 in the flame. In a new study [50] the concentration profiles of various siloxanes were measured during the combustion of methane/air/siloxane gas mixture in the counter-flow configuration, and it was shown that siloxanes decompose completely in the pre-flame and luminous regions within the distance of about 1 mm or less. The combustion can be represented by the following overall reactions

$$CH_4 + 2O_2 \rightarrow CO_2 + 2H_2O \quad (2)$$

$$C_6H_{18}Si_2O + 12O_2 \rightarrow 6CO_2 + 9H_2O + 2SiO_2 \quad (3)$$

At low mole fraction of L2 ($Y_{L2} < 1$) the total number of moles does not change significantly during combustion, therefore the mole fraction of silica molecules Y_0 in combustion products near the burner is estimated as $Y_0 = 2Y_{L2}$. In the present calculations at the inlet the uniform volume concentration of silica molecules $C_0 = Y_0 P/k_B T_0$ is assumed. Here P is the gas pressure in the flame (P = 10^5 Pa) and $T_0 \approx$ 2100 K is the maximum temperature. Silica nanoparticles form and grow due to collisions between SiO_2 molecules and between other silica nanoparticles. These nanoparticles are transported with combustion products. The velocity of combustion products is estimated as V_0 = 1.75 m/s at the maximum temperature and as V = 1.3 m/s at the distance of 75 mm from the burner. Therefore, the particle residence time in the flame $\tau_R \leq 0.06$ s.

Below we will neglect the diffusion of silica particles to macroscopic distances. Silica nanoparticles form a dilute gas mixture in combustion products; and the diffusion of each nanoparticle size class can be considered independently. The main component in combustion products is nitrogen. Therefore, diffusion coefficients of silica nanoparticles can be estimated as a diffusion in a binary mixture of rigid spheres [51]

$$D_k = \frac{1}{3}\sqrt{\frac{2}{\pi}}\sqrt{\frac{1}{m_N}+\frac{1}{k\,m_S}}\,\frac{(k_B T)^{3/2}}{P\pi\left(r_N + r_S k^{1/3}\right)^2}, \quad (4)$$

where $m_{N,S}$ are the mass of nitrogen and silica molecules, $r_{N,S}$ are the radii of nitrogen and silica molecules. According to estimations, for silica nanoparticles the Peclet numbers are high $\mathrm{Pe_k} = VR_b/D_k > VR_b/D_1 = 370$ (where R_b is the burner

radius), i.e. the advection transport dominates the diffusion. For this reason at distances $z \le 75$ mm corresponding to our measurements we will neglect the dilution effect due to silica particle diffusion outside of flame region.

Under the present experimental conditions the flame temperature is close the melting point of silica which is about 2000 K [52]. The size and morphology of silica particles and transition to growth of agglomerates are determined by the rate of collision and the rate of subsequent coalescence or sintering. If particles coalesce faster than they collide then $\tau_f < \tau_c$ and particle collisions result in spherical particles. Here τ_f is the characteristic fusion or sintering time and τ_c is the characteristic collision time. Downstream the flame the particle coalescence is slow compared to the collision rate; and agglomerates of smaller attached particles are produced. Due to sintering the apparent size of these smaller particles (called primary) continue to grow inside the aggregates. Figures 6(a) and 8 show the mean radius and the size distribution of primary particles inside fractal-like agglomerates collected in experiments.

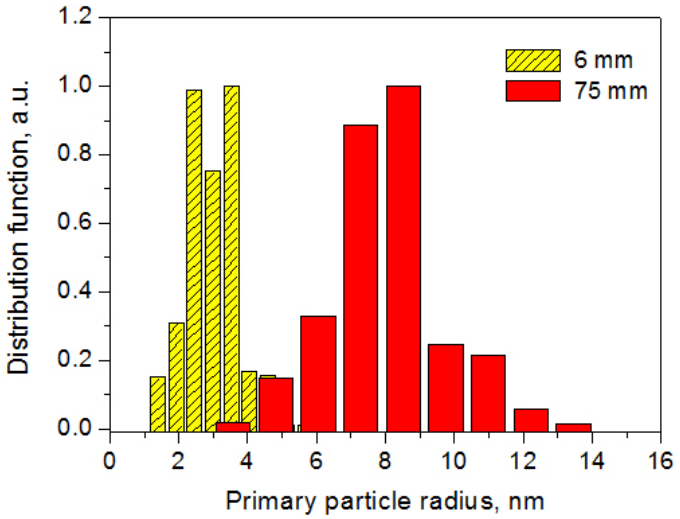

Figure 8 Size distribution of primary particles inside fractal-like agglomerates collected at the distance from the burner 6 mm and 75 mm. L2 concentration is 270 ppm.

Below we estimate the collision and sintering times. It is known that aerosol particles undergoing the Smoluchowski coagulation tend towards an asymptotic self-preserving PSD [19]. In the flame during an initial stage of coagulation the self-preserving size distribution of spherical particles forms very fast. The time to reach the self-preserving distribution starting from rather arbitrary distributions is estimated as [19,53]

$$\tau_{sp} = 5\tau_0 = \frac{5}{C_0}\sqrt{\frac{\rho_S}{6k_B T_0 r_S}} \approx 2\times 10^{-5}\,\mathrm{s}, \quad (5)$$

where τ_0 is the characteristic coagulation time and ρ_S is the silica density. This time can be viewed also as a time required to restore self-preserving distribution if the external conditions change. This time corresponds to a very short distance of 0.035 mm that is smaller than the thickness of the oxidation zone of L2 (about 1 mm, according to Jalali et al. [50]). This means that by the end of L2 oxidation the size distribution of silica particles is already self-preserving, i.e. we can use relations of the corresponding theoretical model [19,54]. After formation of self-preserving distribution the mean volume of silica particles $\bar{v}$ grows with time according to [19,54]

$$\bar{v} = \frac{4\pi}{3} r_S^3 \left(1 + \frac{5\alpha}{12}\frac{t}{\tau_0}\right)^{6/5}, \quad t > \tau_{sp}, \quad (6)$$

where $\alpha \approx 6.6$. Then the characteristic collision time of particles is estimated [19,55] as a characteristic time of change of the mean radius $\bar{R}$

$$\tau_c = \bar{R}\left(\frac{d\bar{R}}{dt}\right)^{-1} \approx 3\bar{v}\left(\frac{d\bar{v}}{dt}\right)^{-1} = \frac{6}{\alpha}\tau_0\left(\frac{\bar{R}}{r_S}\right)^{5/2}. \quad (7)$$

Concerning the coalescence or sintering of nanoparticles, the classical initial stage solid state sintering models for mechanisms such as evaporation-condensation, surface-diffusion, grain boundary diffusion and lattice diffusion are reviewed by Coblenz et al. [56]. The sintering mechanisms of nanoparticles coalescence have been studied extensively, including evaporation–condensation, viscous flow, solid state diffusion and plastic deformation [27,55,57-60].

Following Koch and Friedlander [28] the linear rate law for decrease in the surface area is widely used to model evolution of size distributions of fractal-like particles.

$$\frac{da}{dt} = -\frac{1}{\tau_f}\left(a - a_{sph}\right), \quad (8)$$

where a is the surface area of the agglomerate of primary particles and a_{sph} is the surface area of the spherical particle of the same volume. To describe flame synthesis of non-spherical particles two mechanism of sintering are usually considered. For sintering controlled by bulk diffusion the characteristic coalescence time is given by [60]

$$\tau_f = \frac{k_B T R_p^3}{16\sigma D\omega}, \quad (9)$$

where R_p is the primary particle radius, σ is the surface energy, D is the diffusion coefficient and ω is the molecular volume for diffusion. For sintering by a viscous flow mechanism the characteristic coalescence time is written as [57]

$$\tau_f = \frac{2\eta R_p}{\sigma} \quad , \tag{10}$$

where η is the viscosity.

The primary particle size for silica is typically underpredicted [61-63] based on characteristic coalescence times (9) and (10). A possible reason for discrepancies between the experimental primary particle sizes and model predictions is an uncertainty of physical parameters and/or a dependence of these parameters and transport properties such as atomic diffusivity on particle size.

In the model of this paper we use the experimental measurements of primary particle sizes at high concentration of L2 (270 ppm) in order to infer an effective sintering time. The dependence of primary particle radius on distance z from the burner is well approximated by the dependence

$$R_p^3 = R_{p0}^3 + \beta(z - z_0) \ , \tag{11}$$

where z_0 is the distance from the burner at which fractal-like particles start to form, R_{p0} is the mean radius of primary particles at this distance and β = 7.12x10^{-24} m^2. z_0 can be estimated from the equation $\tau_f = \tau_c$. In the case of high concentration of L2 $z_0 \sim 10^{-2}$ mm.

We define the sintering time as the characteristic time of growth of the mean radius of primary particles

$$\tau_f = R_p \left(\frac{dR_p}{dt} \right)^{-1} = \frac{3R_p^3}{\beta V} \ . \tag{12}$$

Figure 9 shows the ratio of sintering to collision times

$$\frac{\tau_f(R)}{\tau_c(R)} = \frac{\alpha r_S^3}{2\beta V \tau_0} \sqrt{\frac{R}{r_S}} \sim C_0 \sqrt{R} \tag{13}$$

as a function of particle radius for two concentration of L2. In the case of L2 concentration 270 ppm $\tau_f / \tau_c > 1$ at $R > 0.4$ nm, whereas at 50 ppm the sintering time is smaller than the mean collision time or close to it.

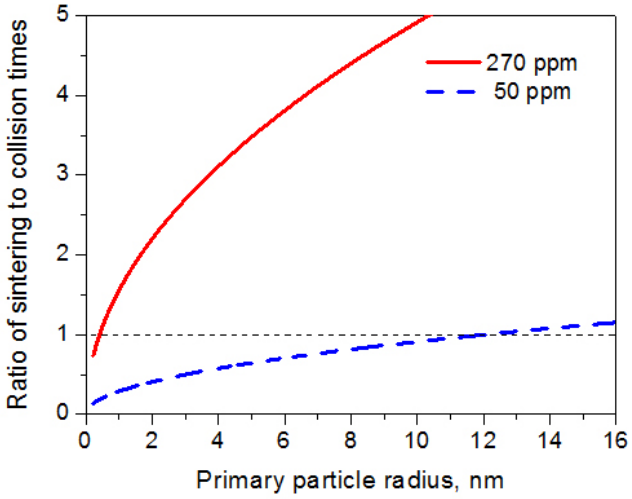

Figure 9 Ratio of sintering to collision times as a function of particle radius for two concentration of L2.

Fig. 9 corresponds with our experimental observation that the majority of silica particles at 50 ppm of L2 are globular. Note that ratio (13) is an increasing function of radius. The linear dependence on radius in Eq. (10) would result in a decreasing function, i.e. in unphysical behavior of the ratio of sintering to collision times.

The cubic dependence on radius may indicate that sintering mechanism is related to bulk diffusion of defects inside silica particles (see Eq. (9)). Below we present arguments in favor of the bulk diffusion mechanism of sintering and propose a new expression for the silica sintering time. Indeed, amorphous silica belongs to a class of strong network-forming liquids [64] in which viscous flow is mediated by diffusion of defects [25,26,65,66]. In amorphous silica the defects are formed by broken silicon-oxygen bonds, which can be considered to be quasi-particles called configurons [26]. In the Doremus model [25,26] the viscosity of amorphous silica is expressed in terms of entropies $S_{f,m}$ and enthalpies $H_{f,m}$ of configuron formation and migration

$$\eta(T) = AT \left[1 + \exp\left(-\frac{S_m}{k_B} + \frac{H_m}{k_B T} \right) \right] \left[1 + \exp\left(-\frac{S_f}{k_B} + \frac{H_f}{k_B T} \right) \right]. \tag{14}$$

This equation with five fitting parameters (A, $S_{f,m}$ and $H_{f,m}$) well describes experimental data in a wide temperature range [66]. The next step is to find the diffusion coefficient of configurons. The configuron effective diffusivity can be estimated using the Eyring expression [67]

$$D = \frac{k_B T}{\lambda \eta}, \tag{15}$$

where λ is the jump distance that has the order of a diameter of diffusing defects. The Eyring equation is similar to the Stokes-Einstein equation describing a moving solid sphere in a continuum viscous liquid. However, for silica and amorphous glasses the Eyring equation is more appropriate because the defect size is close to an atomic size [67,68]

Combining Eqs. (9) and (15) we obtain an estimate for the sintering time

$$\tau_f = \frac{\lambda \eta(T)}{16 \sigma \omega} R_p^3 \tag{16}$$

In our simulations we have found that at a reasonable value of the jump distance $\lambda = 0.5 r_S$ (other parameters are listed in Table I) Eq. (16) produce results very close to those obtained with Eq. (12) derived from experimental data. However, in regard to sintering of silica nanoparticles, it is desirable to test Eq. (16) at other external conditions for silica particle formation (flame temperature and velocity).

Evolution of the ensemble of fractal-like particles can be analyzed by solving a two-dimensional population balance equation for PSD using volume and surface area of particles as

Table I Parameters used for simulation of silica particle formation.

Parameter	*Value*
Mass flux of methane/air mixture, kg/(m^{2}s)	0.28
Pressure, P, Pa	10^5
Flame temperature, T, *K*	$2100\exp(-z/1.42\,\mathrm{m})$
Initial flame velocity, V_0, m/s	1.75
Sticking coefficients, α_{ij}	1
Fractal dimension of large clusters, D_f^{∞}	1.85
w (see Eq. (24))	5
Entropy of defect formation, S_f	$17.54\,k_B$
Entropy of defect migration, S_m	$11.37\,k_B$
Enthalpy of defect formation, H_f, eV	2.456
Enthalpy of defect migration, H_m, eV	5.41
A, Pa·s/K (see Eq. (14))	1.547x10^{-6}
Silica surface energy, σ, J/m^2	0.3
Mean volume of silica molecule, ω, nm^3	0.0464
Mean radius of SiO_2 molecule, r_S, nm	0.223

independent variables [27-29]. In this paper we use one-dimensional approach. The advantage of this approach is that it is based on essentially the same physical assumptions as the two-dimensional approach, but more efficient computationally. To take into account sintering of particles (surface area change), instead of second variable (surface area of particle) we use the dependence of primary particle radius on distance (11) and modify accordingly our one-dimensional model [30]. In the approximation of laminar flow of flue gases, the evolution of the size distribution $C_k(z)$ of silica nanoparticles along the flame axis is described by a set of equations [30] based on the Smoluchowski coagulation equation [18] for the growth of clusters by successive collisions

$$\frac{dVC_1}{dz} = -C_1\sum_{i=1}^{\infty} w_{i,1}C_i\,, \tag{17}$$

$$\frac{dVC_k}{dz} = \frac{1}{2}\sum_{i=1}^{k-1} w_{i,k-i}C_iC_{k-i} - C_k\sum_{i=1}^{\infty} w_{ik}C_i\,, \tag{18}$$

$$C_1\big|_{z=0} = C_0\,, \tag{19}$$

$$C_k\big|_{z=0} = 0\,, \quad k \geq 2\,, \tag{20}$$

where C_k are densities of nanoparticles ($k \geq 1$ is the number of Si atoms in a nanoparticle), V is the particle velocity that is assumed to be the gas flow velocity and w_{ik} is the coagulation kernel [19].

IV. MODELING OF PSD EVOLUTION AND COMPARISON WITH EXPERIMENT

Selection of the coagulation kernel depends on gas phase parameters. In our experiments the mean size of silica agglomerates was less than the mean free path of gas molecules $\lambda_g \sim 400$ nm, i.e. the Knudsen number $Kn = \lambda_g / R_c >> 1$ (R_c is the particle collision radius). For this reason we will use the coagulation kernel for the free molecular regime. At the initial stage of coagulation $\tau_f < \tau_c$ and particles coalesce as fast as they collide, i.e. they grow spherical. The coagulation kernel for spherical particles is given by

$$w_{ij} = \alpha_{ij}\left(R_i + R_j\right)^2\sqrt{\frac{8\pi k_B T}{m_S}\left(\frac{1}{i}+\frac{1}{j}\right)}\,, \tag{21}$$

where $R_i = r_S\sqrt[3]{i}$ is the radius of the particle containing i molecules of SiO_2 and $\alpha_{ij} \leq 1$ is the sticking coefficient accounting for a fact that not all collisions result in particle coalescence [30,69,70]. However, simulation shows that in the problem considered in this paper sticking coefficients do

not influence results signific-antly, because of a fast formation of self-preserving distribution and conservation of particles during this stage (no particle loss because of high Peclet numbers).

When particles travelling through the flame become sufficiently large, at some point τ_f becomes larger than τ_c. Physically this corresponds to the range in the flame where collisions take place more rapidly than sintering. As a result fractal-like aggregates begin to develop. This means that the coagulation kernel (21) for spherical particles is no longer valid. The fractal-like structure significantly affects the frequency of collisions and the rate of coagulation. The morphology of this aggregates can only be characterized at the statistical level by the fractal dimension D_f. We describe collisions between fractal-like particles as collisions between spherical particles each having an effective collision radius [19,33,34]. In our model we define the collision radius R_c of a particle containing k molecules of SiO_2 as

$$R_c(k,x_p) = r_S x_p^{1/3} \left(\frac{k}{x_p}\right)^{\frac{1}{D_f(k,x_p)}}, \qquad (22)$$

where $x_p = \left(R_p/r_S\right)^3$ is the number of SiO_2 molecules in a primary particle.

Since aggregates undergo continuous time- and size-dependent rearrangement as a result of sintering and collisions the fractal dimension $D_f(k,x_p)$ also evolve as a function of number and size of primary particles in an aggregate. For the fractal dimension $D_f(k,x_p)$ we use a simple decreasing function of aggregate size k similar to that we used before [30]

$$D_f(k,x_p) = \begin{cases} 3 & \text{at } k \le x_p \\ D_f^{\infty} + \left(3 - D_f^{\infty}\right)\left[1 + \left(\frac{k - x_p}{w x_p}\right)^2\right]^{-1} & \text{at } k > x_p, \end{cases} \qquad (23)$$

where $D_f^{\infty} = \lim_{k/x_p \to \infty} D_f(k,x_p)$ is the fractal dimension of the large aggregates ($k > x_p$) in the system. The parameter w is responsible for a smooth transition of fractal dimension from $D_f = 3$ (spherical clusters) to $D_f^{\infty} = 1.85$ (fractal-like aggregates). Note that the fractal dimension $D_f(k,x_p)$ depends implicitly on distance z along the flame axis via the dependence of $x_p = \left(R_p/r_S\right)^3$ on z (see Eq. (11)). Equations (22) and (23) describe the whole range of particle sizes. The collision radius of a small spherical particle ($k \le x_p$) coincides with its radius. The collision radius of a fractal-like particle ($k > x_p$) is larger than the radius of the spherical particle with the same number of atoms. In our modeling, instead of coagulation kernel (21) we use the modified coagulation kernel that is appropriate both for small globular clusters and large fractal-like aggregates

$$w_{ij} = \alpha_{ij}\left(R_c(i) + R_c(j)\right)^2 \sqrt{\frac{8\pi k_B T}{m_S}\left(\frac{1}{i} + \frac{1}{j}\right)}. \qquad (24)$$

As can be seen from Eqs. (11) and (22)-(24), in our model the sintering effect is 'hidden' in the coagulation kernel of fractal-like particles via the dependence of primary particle size on distance.

The coagulation equations (17)-(20) were solved numerically by the method described earlier[30] using parameters listed in Table I. At short distances $z \sim 2R_b$ from the burner the gas flow velocity is approximately proportional to temperature $V(z) = T(z)V_0/T_0$. The flame temperature (Fig. 2) is approximated by a simple analytical dependence

$$T(z) = T_0 \exp\left(-z/z_T\right), \qquad (25)$$

where $z_T = 1.43$ m is the characteristic length-scale of temperature change. We start modeling with the coagulation kernel for spherical particles given by Eq. (21). When τ_f becomes larger than τ_c, we switch to the coagulation kernel for fractal-like particles, Eq. (24).

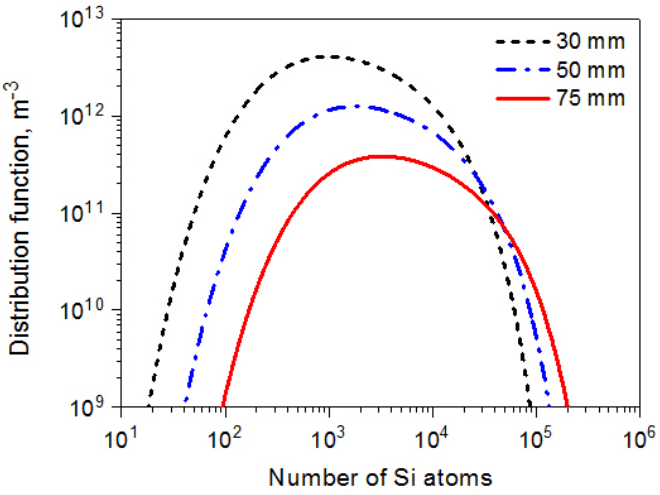

Figure 10 The size distribution of silica particles calculated at L2 concentration 270 ppm.

First, we present modeling results for the case of L2 concentration 50 ppm. Experimentally, in this case the majority of silica particles are globular. Modeling results obtained with both coagulation kernels, Eqs. (21) and (24), are very close. Figure 10 shows the silica PSD as a function of position in the flame. We have found that even though the temperature changes along the flame axis the numerical solution follows the self-preserving solution, i.e. the distribution function can be represented in the form

$$C_k(z) = \Psi(\eta)\frac{N(z)}{\bar{k}(z)} \qquad (26)$$

where $\Psi(\eta)$ depends only on the similarity variable $\eta = k/\bar{k}(z)$, $\bar{k}(z)$ is the mean number of Si atoms in silica particles and $N(z)$ is the total number of particles per unit volume at the distance z from the burner. This result is explained by a very short time needed for formation of self-preserving distribution (see Eq. (5)), i.e. the distribution function of particles travelling with the flue gases adjusts adiabatically to

current conditions.

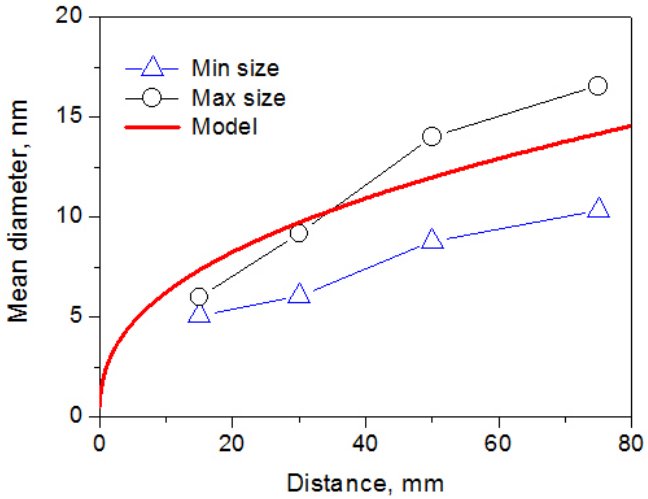

Figure 11 Mean diameter of silica particles (solid line) as a function of the distance from the burner at L2 concentrations 50 ppm. The mean projected length L and width W measured experimentally are shown by symbols.

In Fig. 11 the mean diameter of spherical particles obtained with the model is compared with minimum and maximum sizes of particles measured experimentally. It is seen that the calculated mean radius agrees reasonably well with experimental data.

Modeling results for 270 ppm of L2 are shown in Figs. 12 and 13. The parameter w was varied to obtain a good fit to experimental data. In Fig. 12 the mean collision radius is given by

$$\bar{R}_c(z) = \frac{\sum_k R_c(k, x_p(z)) C_k(z)}{\sum_k C_k(z)} \qquad (27)$$

In order to compare the simulated distributions with the experimental data (Fig. 13) we changed the size variable and defined the size distribution in terms of collision radius

$$F(R_c, z) = \frac{kD_f(k, x_p(z))}{R_c(k, x_p(z))} C_k(z), \quad \int_{r_*}^{\infty} F(r, z)dr = \sum_{k=2}^{\infty} C_k(z). \qquad (28)$$

In Fig. 13 experimental PSDs are plotted as distributions of an approximate collision radius that is defined as the geometric mean

$$R_c^{\exp} = 0.5\sqrt{LW} \qquad (29)$$

From the comparison of simulation results with experimental data it can be concluded that the model captures the essential features of fractal-like particle formation and evolution.

A series of simulations with the same fitting parameters and various temperature profiles lying within the error bars in Fig. 2 have shown that the influence of uncertainty in temperature measurement is small; in both cases of low and high concentration of L2 the PSDs and the mean diameters change only by several percent because of the weak square-root dependence of the coagulation kernels (21) and (24) on temperature. Note also that with a small increase in temperature the residence time of particles in the flame decreases because of increase in the drift velocity V, while the collision rate of particles increases which compensate the residence time decrease. For this reason in our model the overall effect of uncertainty in temperature measurement on evolution of PSD is small.

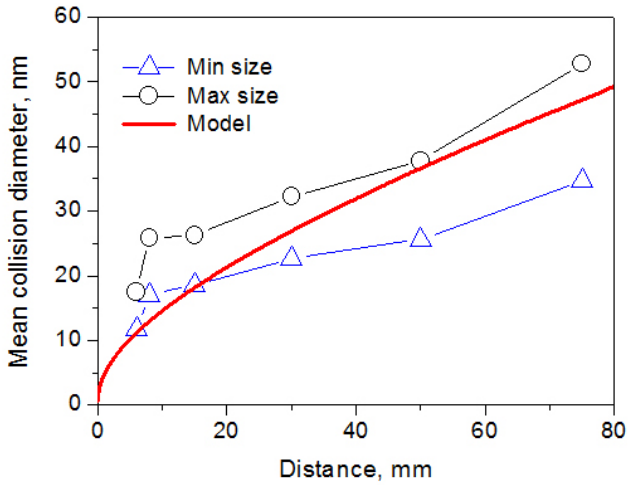

Figure 12 The mean collision diameter $2R_c$ as a function of distance from the burner at L2 concentrations 270 ppm. Comparison with the mean projected length L and width W of fractal-like aggregates.

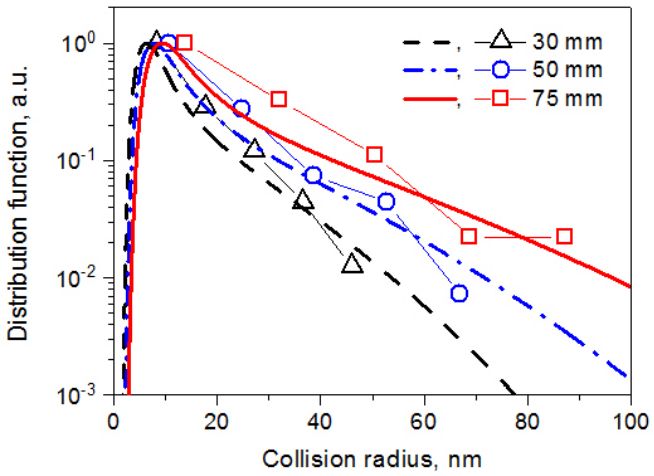

Figure 13 Size distribution of fractal-like aggregates at several distances from the burner. Comparison of model predictions with experimental distributions labeled with symbols. The concentration of L2 is 270 ppm.

V. CONCLUSIONS

(1) Formation of silica fractal-like aggregates during combustion of a stoichiometric methane/air mixture with the hexamethyldisiloxane admixture was studied. TEM analysis of samples taken at various positions in the flame has shown that L2 concentration influences the morphology and size of silica particles. At L2 concentration of 270 ppm random collisions of nanoparticles leads to agglomerates with the fractal-like structure. (2) When travelling downstream, primary particles composing fractal-like aggregates continue to

grow by sintering with neighboring particles. The dependence of primary particle radius on distance z from the burner is approximated by the dependence $R_p^3 \sim \beta z$ The sintering time $\tau_f \sim R_p^3$ derived from this dependence indicates that sintering mechanism is related to bulk diffusion of defects inside silica particle (defect-mediated viscous flow in network-forming materials [25,66]. The new expression for the silica sintering time based on the Doremus model [25,26] of viscosity of amorphous materials has been proposed. (3) Combination of TEM results with the theoretical analysis allowed us to find conditions for formation of silica fractal-like aggregates. The onset of fractal aggregate formation is discussed by studying the characteristic time scales of collisions and coalescence. To simulate the evolution of the size distribution of fractal-like silica particles the one-dimensional Smoluchowski model with size dependent fractal dimension of silica aggregates was formulated. Simulation results demonstrate a good agreement with experimental data. This means that the proposed model is able to capture the effects of the system parameters (such as temperature, gas velocity and L2 concentration) on the onset of silica aggregate formation and evolution of PSD. (4) Since the thickness and density of silica layers formed on internal parts of gas-burning equipment depend on morphology and size distribution of silica particles, the results obtained in this paper are useful for elaboration of siloxane/silicon specifications for equipment utilizing biogas.

VI. ACKNOWLEDGEMENTS

The Netherlands Organization for Scientific Research NWO is acknowledged for financial support of one of the authors (A.A.T.).

VII. REFERENCES

[1] P. Roth, Proc. Combust. Inst. **31**, 1773 (2007).
[2] S. E. Pratsinis, Prog. Energy Combust. Sci. **24**, 197 (1998).
[3] M. S. Wooldridge, Prog. Energy Combust. Sci. **24**, 63 (1998).
[4] L. Madler, H. K. Kammler, R. Mueller, and S. E. Pratsinis, J. Aerosol Sci. **33**, 369 (2002).
[5] W. J. Stark and S. E. Pratsinis, Powder Technol. **126**, 103 (2002).
[6] D. E. Rosner, Ind. Eng. Chem. Res. **44**, 6045 (2005).
[7] R. Strobel, S.E. Pratsinis, J. Mater. Chem. **17**, 4743 (2007).
[8] R. Dewil, L. Appels, and S. J. Baeyen, Energy Convers. Manage. **47** 1711 (2006).
[9] E. Wheless and J. Pierce, in *Proceedings of SWANA's 27th Annual Landfill Gas Symposium,* San Antonio, Texas, 22-25 March 2004.
[10] N. Nair, X. Zhang, J. Gutierrez, J. Chen, F. Egolfopoulos, and T. Tsotsis, Ind. Eng. Chem. Res. **51**, 15786 (2012).
[11] N. Nair, A. Vas, T. Zhu, W. Sun, J. Gutierrez, J. Chen, F. Egolfopoulos, and T. Tsotsis, Ind. Eng. Chem. Res. **52**, 6253 (2013).
[12] E. A. McBean, Can. J. Civ. Eng. **35**, 431 (2008).
[13] A. A. Turkin, M. Dutka, D. Vainchtein, S. Gersen, V. M. van Essen, P. Visser, A. V. Mokhov, H. B. Levinsky, and J. Th. M. De Hosson, Appl. Energy **113**, 1141 (2014).
[14] O. Sevimoğlu and B. Tansel, Waste Manage. **33**, 74 (2013).
[15] W. Urban, H. Lohmann, and J. J. S. Gomez, J. Power Sources, 193, 359 (2009).
[16] P. Huguen and G. Le Saux, *Perspectives for a European standard on biomethane,* 2010, see http://www.biogasmax.eu/media/d3_8_new_lmcu_bgx_eu_standard_14dec10_vf__077238500_0948_26012011.pdf
[17] B. M. Smirnov, M. Dutka, V. M. van Essen, S. Gersen, P. Visser, D. Vainchtein , J. Th. M. De Hosson, H. B. Levinsky, and A. V. Mokhov, Europhys. Lett. **98**, 66005 (2012).
[18] M. V. Smoluchowski, Z. Phys. Chem. **92**, 129 (1917).
[19] S. K. Friedlander, *Smoke, Dust and Haze: Fundamentals of Aerosol Dynamics,* 2nd edn. (Oxford University Press, 2000).
[20] S. R. Forrest and T. A. Witten Jr, J. Phys. A: Math. Gen. **12** L109 (1979).
[21] R. D. Mountain, G. W. Mulholland, and H. Baum, J. Colloid Interface Sci. **114**, 67 (1986).
[22] G. W. Mulholland, R. J. Samson, R. D. Mountain, and M. H. Ernsts, Energy and Fuels, **2**, 481 (1988)
[23] C. M. Sorensen, Aerosol Sci. Technol. **45**, 765 (2011)
[24] M. L. Eggersdorfer and S. E. Pratsinis, Aerosol Sci. Technol. **46**, 347 (2012).
[25] R. H. Doremus, J. Appl. Phys. **92**, 7619 (2002).
[26] M. I. Ojovan, K. P. Travis, and R. J. Hand, J. Phys.: Condens. Matter, **19**, 415107 (2007).
[27] Y. Xiong, M. K. Akhtar, S. E. Pratsinis, J. Aerosol Sci. **24**, 301 (1993)
[28] W. Koch and S. K. Friedlander, J. Colloid Interface Sci. **140**, 419 (1990).
[29] Y. Xiong and S. E. Pratsinis, J. Aerosol Sci. **24**, 300 (1993).
[30] A. A. Turkin, M. V. Dutka, Y. T. Pei, D. I. Vainshtein, and J. Th. M. De Hosson, J. Appl. Phys. **111**, 124326 (2012).
[31] P. Meakin, *Fractals, Scaling and Growth Far from Equilibrium* (Cambridge University Press, Cambridge, 1998).
[32] Ü. Ö. Köylü and G. M. Faeth, Combust. Flame **89**, 140 (1992).
[33] T. Matsoukas and S. K. Friedlander, J. Colloid Interface Sci. **146,** 495 (1991).
[34] M. K. Wu and S. K. Friedlander, J. Aerosol Sci. **24**, 273 (1993).
[35] A. V. Mokhov and H. B. Levinsky, Proc. Combust. Inst. **28**, 2474 (2000).
[36] D. A. Stephenson and R. J. Blint, Appl.

Spectroscopy **33**, 41 (1979).
[37] M. D. Allendorf, J. R. Bautista and E. Potkay, J. Appl. Phys. **66**, 5046 (1989).
[38] A. Mokhov, S. Gersen, and H. Levinsky, Chem. Phys. Lett. **403**, 233 (2005).
[39] R. J. Kee, F. M. Rupley, and J. M. Miller, *CHEMKIN II: A Fortran Chemical Kinetics Package for the Analysis of Gas-Phase Chemical Kinetics* (Sandia National Laboratories, 1989).
[40] GRI-Mech 3.0 (see: http://www.me.berkeley.edu/gri_mech/)
[41] J. Lee, I. Altman, and M. Choi, J. Aerosol Sci. **39**, 418 (2008).
[42] L. Waldmann and K. H. Schmitt, in *Aerosol Science* edited by C. N. Davies (Academic Press, London, 1966) p. 137.
[43] D. E. Rosner and Y. F. Khalil, J. Aerosol Sci. **31**, 273 (2000).
[44] A. Messerer, R. Niessner, and U. Pöschl, J. Aerosol Sci. **34**, 1009 (2003).
[45] D. W. Mackowski, J. Aerosol Sci. **37**, 242 (2006).
[46] M. Zurita-Gotor, J. Aerosol Sci. **37**, 283 (2006).
[47] D. Boldridge, J. Aerosol Sci. **44**, 1821 (2010).
[48] P. Soille, *Morphological Image Analysis: Principles and Applications* (Springer-Verlag New York, 2003).
[49] J. Warnatz, U. Maas, and R.W. Dibble, *Combustion,* 4th edn. (Springer Berlin, 2006).
[50] A. Jalali, N. Liu, M. M. Yousef Motamedhashemi, F. Egolfopoulos, and T. Tsotsis, Combust. Sci. Technol. **185**, 953 (2013)
[51] R. B. Bird, W. E. Stewart, and E. N. Lightfoot, *Transport Phenomena* (Wiley, New York, 1960).
[52] *Handbook of Chemistry and Physics*, Vol. **86**, edited by D. R. Lide (CRC Press, London, 2003–2004).
[53] S. Vernury, K. A. Kusters, and S. E. Pratsinis, J. Colloid Interface Sci. **165**, 53 (1994).
[54] F. S. Lai, S. K. Friedlander, J. Pich, and G. Hidy, J. Colloid Interface Sci. **39**, 395 (1972).
[55] K. E. J. Lehtinen, R. S. Windeler, S. K. Friedlander, J. Aerosol Sci. **27**, 883 (1996).
[56] W. S. Coblenz, J. M. Dynys, R. M. Cannon, and R. L. Coble, Mater. Sci. Res. **13**, 141 (1980).
[57] J. Frenkel, J. Phys. USSR, **9**, 385 (1945).
[58] G. D. Ulrich and J. W. Riehl, J. Colloid Interface Sci. **87**, 257 (1982).
[59] P. P. Bolsaitis, J. F. McCarthy, G. Mohiuddin, and J. F. Elliott, Aerosol Sci. Technol. **6**, 225 (1987).
[60] S. K. Friedlander and M. K. Wu, Phys. Rev. B, **49**, 3622 (1994).
[61] S. H. Ehrman, S. K. Friedlander, and M. R. Zachariah, J. Aerosol Sci. **29**, 687 (1998).
[62] S. H. Ehrman, J. Colloid and Interface Sci. **213**, 258 (1999).
[63] I. V. Schweigert, K. E. J. Lehtinen, M. J. Carrier, and M. R. Zachariah, Phys. Rev. B, **65** 235410 (2002).
[64] C. A. Angel, J. Non-Cryst. Solids, **131-133**, 13 (1991).
[65] N. F. Mott, Philos. Mag. B **56**, 257 (1987).
[66] M. I. Ojovan and W. E. Lee, J. Appl. Phys. **95**, 3803 (2004).
[67] H. Eyring, J. Chem. Phys. **4**, 283 (1936).
[68] M. L. F. Nascimento and E. D. Zanotto, Phys. Rev. B, **73**, 024209 (2006).
[69] D. L. Bunker, J. Chem. Phys. **32,** 1001 (1960).
[70] B. Briehl and H. M. Urbassek, J. Vac. Sci. Techn. A, **17**, 256 (1999).